Varano, E., Zhou, M., Lanham, S., Iredale, R. J., van Duijneveldt, J. S., & Hamerton, I. (2019). Developing toughened bismaleimide-clay nanocomposites: Comparing the use of platelet and rod-like nanoclays. *Reactive and Functional Polymers*, *134*, 10-21. https://doi.org/10.1016/j.reactfunctpolym.2018.10.006

Developing toughened bismaleimide-clay nanocomposites: comparing the use of platelet and rod-like nanoclays.

Enrico Varano[1], Ming Zhou[1], Samuel Lanham[1], Robert J. Iredale[1], Jeroen S. van Duijneveldt[2], and Ian Hamerton[1,]*

[1]Bristol Composites Institute (ACCIS), Department of Aerospace Engineering, School of Civil, Aerospace, and Mechanical Engineering, Queen's Building, University Walk, University of Bristol, Bristol, BS8 1TR, U.K.

[2]School of Chemistry, Cantock's Close, University of Bristol, Bristol, BS8 1TS, U.K.

Supplementary Information

Solution blending

Measured quantities of the clays were dried under vacuum (50°C, overnight) and stored in sealed test tubes. Weight measurements indicated water contents between 5% and 10% were present before drying, confirming the need for the drying process and sealed storage. An IKA® Ultra TURRAX T-18® high shear mixer was used to aid the dispersion of 4.4 wt% clays and 50 wt% BMI in separate DMF solutions (5 minutes at 20k rpm); in a small number of cases a polyisobutylene-based dispersant (SAP 230 TP) was added to evaluate the effect. The clay solutions were then blended with the BMI using a magnetic stirrer (Table S1). All concentrations below are expressed as weight percentages.

Table S1. Sample designations for the DMF solution blends studied in this work.

Sample	Compimide 200 (wt%)	Montmorillonite	Sepiolite	
		SWy-2 (wt%)	Pangel B20 (wt%)	Pangel B40 (wt%)
BMI-0_S	50	-	-	-
$SWy2_S$	-	4.4	-	-
$B20_S$	-	-	4.4	-
$B40_S$	-	-	-	4.4
BMI-$SWy2_S$	25	2.2	-	-
BMI-$B20_S$	25	-	2.2	-
BMI-$B40_S$	25	-	-	2.2

In order to analyse the dispersions, samples (1 μL) were taken and dried on microscope slides and SEM sample stands to form gel films. Thicker films were cast in order to attempt cure of the BMI. The samples were made by casting the solutions in a silicone mould ($3 \times 15 \times 100$ mm^3 – see Fig. S1) and allowing the DMF to evaporate in a fume cupboard over 48 hours. Attempts were made at drying the samples under 50°C vacuum overnight.

Figure S1. BMI-0_S cast in silicone moulds

Cure schedule

The solution blends and films (Table S2) were cured using the following procedure. Samples were first molten at 140 ˚C for 30 minutes and then degassed for 10 minutes to reduce heat-induced voids. The temperature was then raised at 4 K min^{-1} to the curing temperature of 180 ˚C before being held isothermally for 1 hour. A post-cure temperature of 200 ˚C (30 minutes) was then performed before cooling the samples at a rate of 5 K min^{-1} to room temperature.

Table S2. Sample designations for the dry film blends studied in this work.

Sample	Compimide 200 (wt%)	Montmorillonite	Sepiolite	
		SWy-2 (wt%)	Pangel B20 (wt%)	Pangel B40 (wt%)
BMI-0_F	100	-	-	-
BMI-$SWy2_F$	91.9	8.1	-	-
BMI-$B20_F$	91.9	-	8.1	
BMI-$B40_F$	91.9	-	-	8.1

Microscopy

Powdered BMI samples and films of dried DMF solution were observed using an Olympus BX51 microscope with a CMOS colour camera (Pixelink PL-B625CU). Particle size distributions were measured and compared by Image Processing and Analysis by Java 1.6.0 (Image J). The dried solution films were analysed using a Jeol JSM-IT300 scanning electron microscope (SEM) operating at an accelerating voltage of 15 kV.

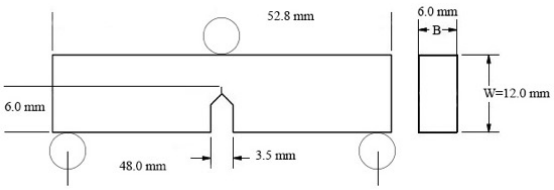

Figure S2. Test configuration of single etch notched beam (SENB).

Investigating the stability of the clays within the BMI

Despite the suspected difficulties in removing the DMF, it was deemed worthwhile to investigate the compatibility of the BMI and clays in solution as this approach allowed for more controlled mixing and therefore even clay exfoliation. This preliminary work is performed as a control to study the compatibility of the clays with the BMI and to determine which clay is best suited to this particular system. The BMI-0_S, SWy2_S, B20_S, and B40_S samples were prepared to verify to what extent the BMI and the clays are soluble in DMF. It was found that the BMI-0_S sample containing 50 wt% BMI was supersaturated and would precipitate within minutes. The 4.4 wt% SWy-2 in the SWy2_S sample quickly precipitated showing the very limited solubility of the phyllosilicate clay while B20_S and B40_S proved to be stable gels, particularly in the presence of SAP 230 TP, which also led to smoother SEM images.

A degree of chemical compatibility between the BMI and clays was confirmed by the BMI-SWy2_S, BMI-B20_S, and BMI-B40_S samples: mixing the BMI dispersion with the clay solutions in equal parts anecdotally created stronger gels despite the reduction in relative solute concentration. The 2.2 wt% montmorillonite BMI-SWy2_S sample was a stable suspension for up to two hours while no precipitate or phase separation was recorded for the BMI-B20_S and BMI-B40_S samples. SEM image analysis and microscopic observations of the 1 mm thick, dried gel films (BMI-0_F, BMI-

SWy2$_F$, BMI-B20$_F$, and BMI-B40$_F$) were performed in order to compare the effects of different fillers on the level of dispersion. The BMI homopolymer (BMI-0$_F$) displays birefringent aggregates, presumably due to microcrystalline deposits or fine bubbles. The addition of the clay particles reduces the number and density of birefringent species in the gel film (Fig. S3) in particular, the BMI-B40$_F$ sample showed a remarkably good dispersion – a result that was corroborated with the SEM images[1] (Fig. S4), BMI-B40$_F$ is the sample with the smallest features. Based on the foregoing measurements, it was decided that the Pangel B40 organoclay, modified for high polarity systems, would be best suited for further work aiming at analysing the thermo-mechanical properties of a clay-BMI nanocomposite.

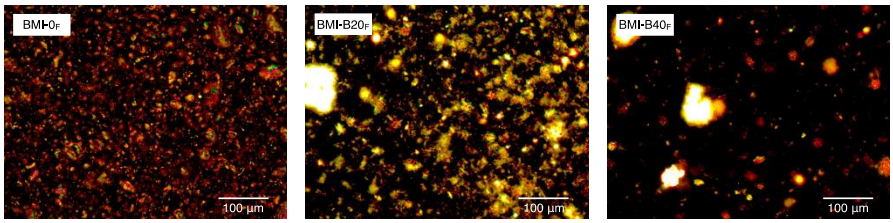

Figure S3. Dried gel film polarised light micrographs (magnification 20x) showing the reduction in the number of birefringent aggregates when sepiolite clays are added to BMI.

[1] It was not possible to include the BMI-SWy2$_F$ sample in the micrograph study and the BMI-0$_F$ sample in the SEM study as the gels they formed were not stable enough to allow for even drying.

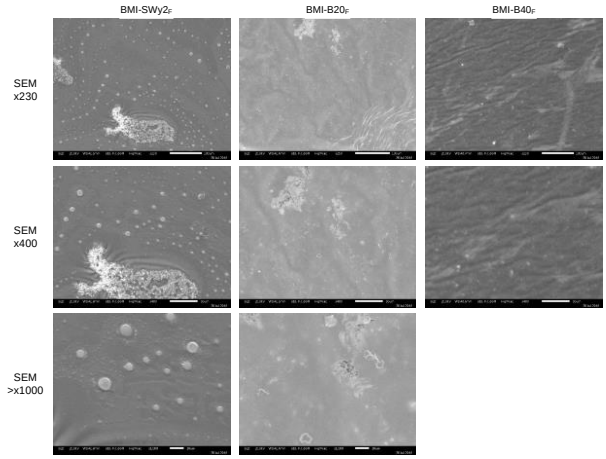

Figure S4. Dried gel film Scanning Electron Microscope (at varying magnifications) showing the reduced number of aggregates when sepiolite clays are added to BMI compared to the effect of the phyllosilicate clay.

Investigating the feasibility of solution vs. solid state blending

Initial work was carried out to investigate whether a good degree of molecular affinity is present between the BMI and the sepiolite clays and, having obtained positive results, several attempts were undertaken to dry larger samples of BMI-0_S and BMI-$B40_S$. It was observed that a dry, impermeable, skin-like layer formed on the surface of the samples, inhibiting the evaporation of the DMF from the rest of the sample. Several attempts at extracting the DMF in a vacuum oven were undertaken unsuccessfully and the resulting uneven pastes still contained at least 20 wt% DMF. Attempts were made at hand moulding the tough paste and curing as per the shorter cure cycle. It was noted that the surface of the samples cured quickly, forming an impermeable layer through which any residual DMF present in the samples was enclosed. The resulting cured specimens were therefore highly porous (Fig. S5).

Figure S5. Porous cured BMI specimens.

Table S3 FTIR absorbance spectrum of Compimide 200 (BMI-0) and proposed assignments.

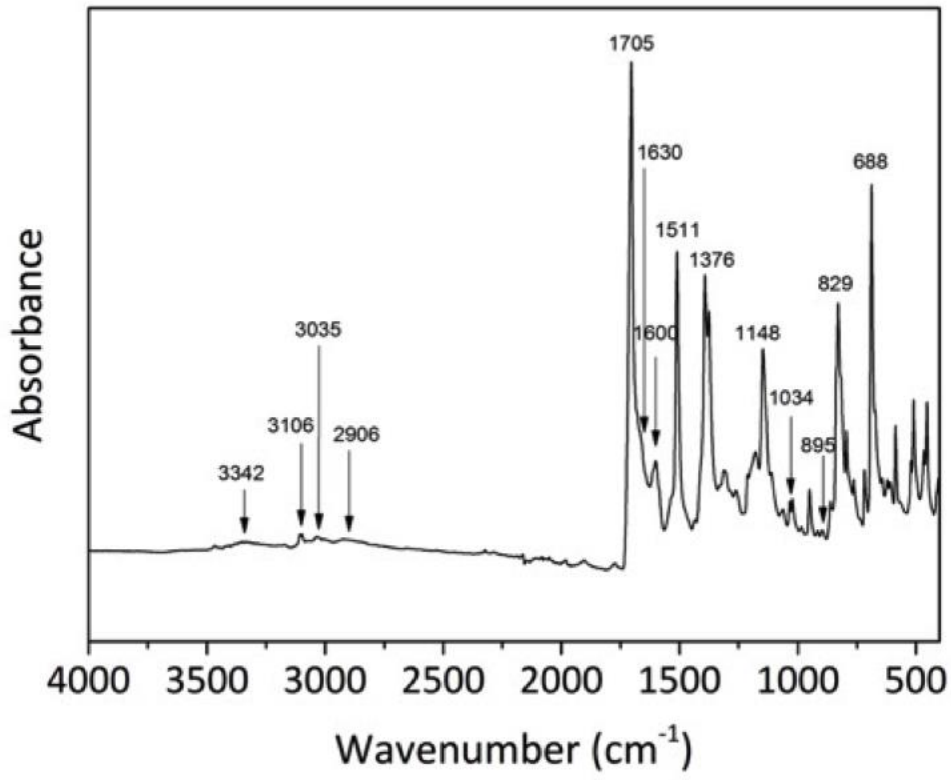

Wavenumber (cm^{-1})	Proposed assignment
3342	N-H stretch (secondary amine)
3106	=C-H stretch (maleimide ring)
3035	Ar-H stretch (phenyl ring)
2906	C-H stretch (methylene)
1705	C=O stretch (maleimide and succinimide rings)

1630	C=C stretch (maleimide ring)
1600	C--C stretch (phenyl ring)
1511	C--C stretch (phenyl ring)
1376	O=C-N stretch (maleimide and succinimide rings)
1148	C-N-C stretch (maleimide and succinimide rings)
1034, 1022	Ar-H in plane deformation (phenyl ring)
895	=CH out of plane deformation (maleimide ring)
829	Ar-H out of plane deformation (1,4-disubstituted phenyl ring)
688	Ar-H out of plane deformation (1,4-disubstituted phenyl ring)

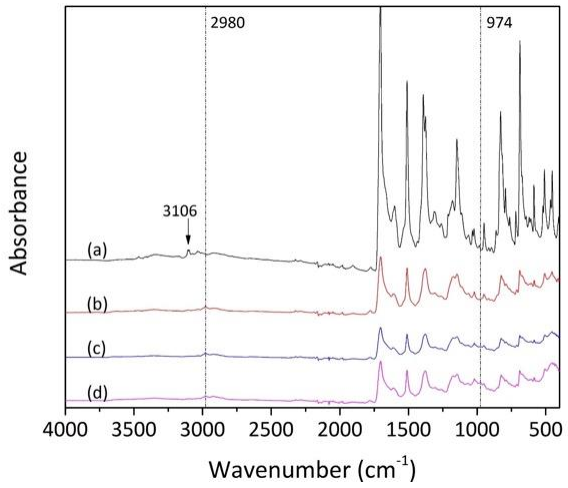

Figure S6. FTIR absorbance spectra for (a) neat BMI-0 monomer, (b) cured BMI-0, and cured BMI nanocomposites (c) BMI-B40$_{2.5b}$ and (d) BMI-B40$_{5b}$. Note spectra are offset for clarity.

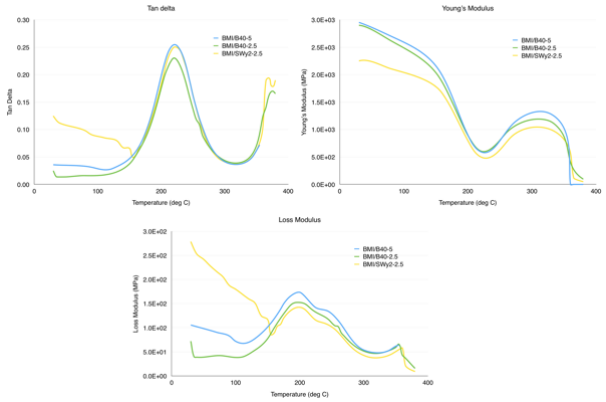

Figure S7. DMTA data for BMI-B40$_{5b}$ (blue), BMI-B40$_{2.5b}$ (green), and BMI-SWy2$_{2.5b}$ (yellow) as a function of temperature.

Table S4. Selected thermal and thermo-mechanical properties for cured neat resins.

Resin	E’ at 100 °C (MPa)	E’ onset	E’’ peak	tan(δ) peak
BMI-0	1360	152	217	178
BMI-B40$_{2.5b}$	1477	160	207	169
BMI-B40$_{5b}$	1465	158	211	172

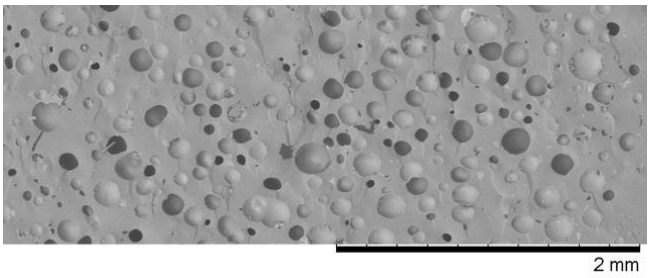

Figure S8. SEM image of air bubbles through the thickness of a cured sample of BMI-SWy3$_{2.5b}$.

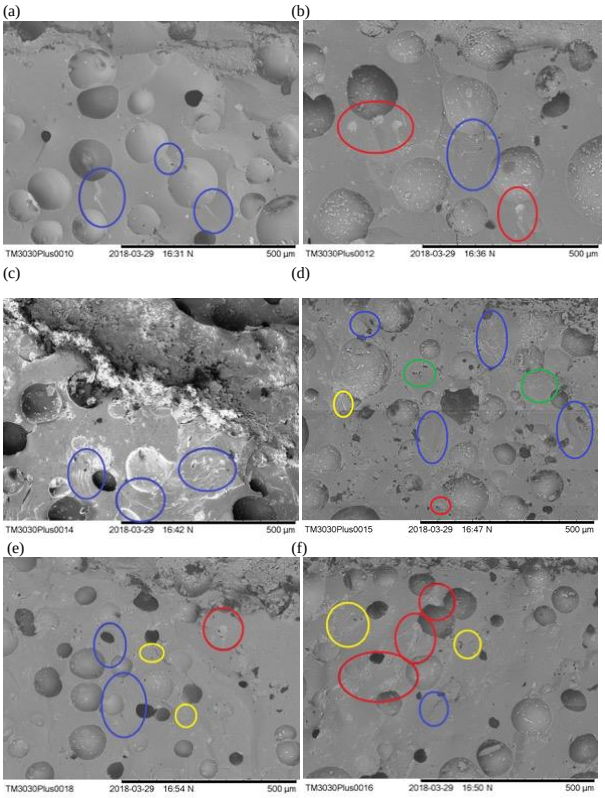

Figure S9. SEM images of fractured surfaces of (a) BMI-SWy3$_{2.5b}$, (b) BMI-SWy3$_{5b}$, (c) BMI-B20$_{2.5b}$, (d) BMI-B20$_{5b}$, (e) BMI-B40$_{2.5b}$ and (f) BMI-B40$_{5b}$. The features highlighted are scarps (blue circles), parabolas (green circles), ribbons (yellow circles), and wrenched clay tactoids (red circles).